Journal of Rock Mechanics and Geotechnical Engineering 11 (2019) 146–158

Contents lists available at ScienceDirect

Journal of Rock Mechanics and Geotechnical Engineering

journal homepage: www.rockgeotech.org

Full Length Article

Investigation of rockfall-prone road cut slope near Lengpui Airport, Mizoram, India

A.K. Verma [a], Sahil Sardana [b,*], Pushpendra Sharma [c], Lal Dinpuia [d], T.N. Singh [e]

[a] Department of Mining Engineering, Indian Institute of Technology (Banaras Hindu Universiy), Varanasi, Uttar Pradesh, 221005, India
[b] Department of Mining Engineering, Indian Institute of Technology (Indian School of Mines), Dhanbad, Jharkhand, 826004, India
[c] Department of Civil Engineering, Lassonde School of Engineering, York University, Toronto, Canada
[d] Department of Geology, Pachhunga University College, Aizawl, Mizoram, 796001, India
[e] Department of Earth Sciences, Indian Institute of Technology Bombay, Mumbai, Maharashtra, 400076, India

ARTICLE INFO

Article history:
Received 16 January 2018
Received in revised form
24 May 2018
Accepted 25 July 2018
Available online 2 December 2018

Keywords:
Rockfall hazards
Rockfall simulation
Rockfall hazard rating system (RHRS)
Road cut slopes
Slope stability

ABSTRACT

Rockfall is one of severe natural hazards that are frequently reported in northeast region of India. It carries rock block falling from the cliff with high velocities and energies which can result in damages to vehicles, disruption to transportation, injuries and fatalities. The massive rockfall event which occurred in April 2017 on the highway NH-44A, near Lengpui Airport, blocked the traffic for 1 d, and fortunately, no casualties were reported as the event occurred in the night. This is the only highway connecting the Aizawl city to the airport and the region is highly prone to rockfall events. Hence assessment of rockfall along this highway is necessary. In the current study, rockfall hazard assessment has been carried out on three locations by rockfall hazard rating system (RHRS). During pre-failure analysis, the result shows that most hazardous slopes have RHRS score of 639. The slopes were found to be vulnerable and later on the rockfall activity occurred. Three-dimensional (3D) stability analysis has been carried out using 3DEC software package to analyze the failure behavior and to decide the rockfall-prone zone (unstable blocks) for slope. The total displacement of 2.24 cm and velocity of 2.25 mm/s of the failed block have been observed in the numerical analysis. Further, the rockfall vulnerable zone (unstable blocks) is considered to determine the parameters such as run-out distance, bounce height and energies of the falling rock blocks. The maximum total kinetic energy of 5047 kJ has been observed in the numerical analysis with the maximum run-out distance up to 18 m.

1. Introduction

Rockfall and other types of landslides are the critical problems in the northeast region of India, especially at the time of rainy season. Over past few decades, many minor and major rockfalls and slides have been reported in this area (Lallianthanga et al., 2013). Rockfall is the fastest type of landslide in which individual or several rock blocks are detached from the surface of the slopes and fall downwards due to gravity effect (Cruden and Varnes, 1996). It is a rapid process and very common in the mountainous region. The high velocities and energies associated with rockfall result in loss of life, and damages to infrastructures and vehicles. Rockfall has been classified on the basis of volume or size of falling rock blocks. Weathering, fracturing and opening of joints in the bedrock of slope increase the probability of occurrence of rockfall. The morphological and geotechnical properties of the bedrock slope also affect the rockfall frequency (Douglas, 1980; Dorren, 2003). The primary causes of rockfall are rain storms (Wei et al., 2014; Wieczorek et al., 1995, 2000), freeze–thaw cycle (McCarroll et al., 1998; Matsuoka and Sakai, 1999), seismic activities (Valagussa et al., 2014) and root penetration. According to the rainfall data, the average rainfall of 100 in (254 cm) per year occurred in the Aizawl city which can trigger the rockfall activity. Unplanned excavation for roadways and human intervention are the minor factors in comparison with other factors (Wieczorek and Jager, 1996). The modes of motion followed by detached rock blocks are fall, roll, bounce and slide. The motion of the rock blocks depends on the parameters such as slope height, slope geometry, slope angle and shape of the rock blocks (Ritchie, 1963). The slopes on the highway NH-44A are

* Corresponding author.
E-mail address: sahilsardana.ymca@gmail.com (S. Sardana).
Peer review under responsibility of Institute of Rock and Soil Mechanics, Chinese Academy of Sciences.

https://doi.org/10.1016/j.jrmge.2018.07.007

vertical or sub-vertical; thus the probability of falling motion of rock block is higher. The falling motion further transforms into bounce motion after hitting at the roadway. During the bounce, rock block strikes at the slope surface and loses its more than 75% of energy, which is gained during the initial rock fall (Evans and Hungr, 1993). The magnitude of kinetic energy is high during falling motion as compared to other modes of motion. This makes the rockfall very severe and to prevent it, analysis of rockfall is necessary for the populous region (Verma and Singh, 2010; Sarkar et al., 2016).

Rockfall hazard is a concern to the probability of rockfall of a given volume within a specified region and time (Varnes, 1984; Guzzetti et al., 1999). The concept of rockfall hazard assessment was pioneered by Brawner and Wyllie (1976) for the Canadian Pacific Railways. Rockfall hazard rating system (RHRS) was developed by Oregon Department of Transportation (ODOT) to assess the rockfall hazard along the highways in Oregon (Pierson et al., 1990; Pierson and Van Vickle, 1993). RHRS was one of the early methods for assessment of rockfall hazards. It is a qualitative method which further leads to the development of various rockfall hazard assessment methods. The RHRS score can be divided into two ratings: hazard and risk ratings by using the same parameters (Fell et al., 2008; Wyllie, 2014). The parameters such as slope height, geological character, rock block size/volume, climate conditions and rockfall history can be associated with hazard rating whereas ditch effectiveness, traffic conditions and road conditions can be related to risk ratings (Budetta, 2004). The main limitation of RHRS is that the final ratings depend on the skill of the field operator and the terminology can be taken in a different way which makes the final RHRS ratings hardly reproducible (Vandewater et al., 2005; Ferrari et al., 2016). The concept of energy was not included in these parameters either. Different statistical and deterministic approaches have been applied for the assessment of rockfall hazards (Guzzetti et al., 2006; Sardana and Verma, 2017). Rockfall hazard assessment has been carried out for the protection of historical structures (Wang et al., 2012), effects on the forest (Perret et al., 2004; Dorren et al., 2006) and along the highway cut slopes (Ansari et al., 2016). A number of rockfall simulations (Ansari et al., 2012; Ahmad et al., 2013; Singh et al., 2013; Sardana et al., 2017; Verma et al., 2018) and stabilities of road cut slopes (Singh and Verma, 2007; Sarkar et al., 2012; Verma et al., 2016; Kundu et al., 2017; Kumar et al., 2018) have been carried out by many researchers in India. The rockfall simulation evaluates the parameters such as bounce height, velocity, kinetic energy and maximum run-out distance. These parameters are further used for the selection of protective measurement such as rock barriers, rock sheds, retaining walls and net. The trajectory of falling rock blocks plays a crucial role in the understanding of road cut slopes. The trajectory of rockfall is affected by the factors such as sources of rockfall, size and shape of rock blocks and properties of slope material (Agliardi and Crosta, 2003). Stability of the slope, as well as rockfall vulnerable zone, has been examined and analyzed using the three-dimensional (3D) distinct element method (DEM). The DEM introduced by Cundall (1988) has the capability to include a large number of rock joints explicitly. In the DEM, the rock mass is considered as an assembly of different intact rock blocks. The joints between intact blocks are treated as boundary conditions. The displacement and contact force at the boundaries of stressed intact blocks are evaluated from the movements of intact block assembly in previous steps. This translational and rotational movement of block assembly is caused by the application of body and boundary forces. Many researchers have considered this approach in the numerical analysis of slope stability, jointed rock mass and arch dams stability problems (Zhang et al., 2006; Jin et al., 2011).

In the present study, the RHRS has been used for the assessment of the rockfall hazards. Though RHRS is a classical approach, all the parameters which are presently used in the explanation of rockfall hazard are considered in this approach. Apart from the rockfall hazard, the 3D stability analysis has been carried out for the studied slope and its findings have been further used in the analysis of rockfall. The rockfall simulation has been carried out by using Rocfall 5.0 for the analysis of bounce height, maximum run-out distance, trajectories, velocity and intensity of falling rock block. The road which connects the Lengpui Airport to the Aizawl city has witnessed many rockfall events. The high intensity of the rainfall on the steep slopes initiates the rockfall. The massive rockfall that occurred on NH-44A near Lengpui Airport in April 2017 cut off the city from the airport as rockfall triggered by heavy pre-monsoon rain blocked the national highway. Even though this region has suffered many rockfall events and landslides in the past few decades, only a limited rockfall study has been carried out by the researchers in this region. The combination of RHRS method and rockfall simulation may help in identification of hazardous slope and then analyzing the bounce height and kinetic energy of falling rock blocks for that slope. The necessity of safe transportation through the vulnerable road cut slopes makes the assessment of rockfall in this route imperative. The proper construction and maintenance of roadway and other infrastructures are a great challenge in rockfall-prone area which makes this study necessary. The main objective of this study is to assess the rockfall vulnerability by RHRS and equation of motions along with the 3D stability so that a proper remedial measure can be implemented against the rockfall which makes the roadway safer for society.

2. Study area

The studied locations are located on the highway NH-44A, from the Lengpui Airport to the Aizawl city. The locations (L-1, L-2 and L-3) are 3.7 km, 4.9 km and 12.7 km away from the airport towards the city, respectively (Fig. 1). The coordinates of the studied slope are N23°49′09.00″ to N23°48′27.23″ and E92°37′32.00″ to E92°39′40.01″ and it comes under toposheet number 84A/9 of the survey of India. The map of the studied locations is shown in Fig. 1. General geology around the Aizawl district is composed of sedimentary rocks of Barail group, Bhuban group, Surma group and Tipam formation (Kesari, 2011). The Barail group comprises shale interbedded with siltstone and covers the eastern part whereas the western part is covered by Bhuban formation. The Bhuban formation is arenaceous, described mostly by thick sandstone beds, and is compact, hard and medium- to fine-grained and grey to khaki colored. The formation of the road cut slopes on NH-44A is composed of sandstone, siltstone and/or shale.

The location L-1 comprises of sandstone with thin shale bedding. The massive sandstone blocks were over-hanging on the underlying soft shale. The heights of the massive sandstone blocks and shale bedding are 18 m and 12 m, respectively. This is the main cause of differential weathering during a rainy season. The field photograph shows five massive sandstone blocks lying on shale bedding before failure (Fig. 2a). A large opening of joints has been observed between the two massive sandstone blocks. After the failure of sandstone block, the large boulders with height of 2.5 m fell down from the slope and blocked the roadway (Fig. 2b).

3. Methodology

In this study, RHRS has been applied to the road cut slopes for the evaluation of rockfall hazard. The survey has been done before the failure occurred at the studied location. The detailed rating of

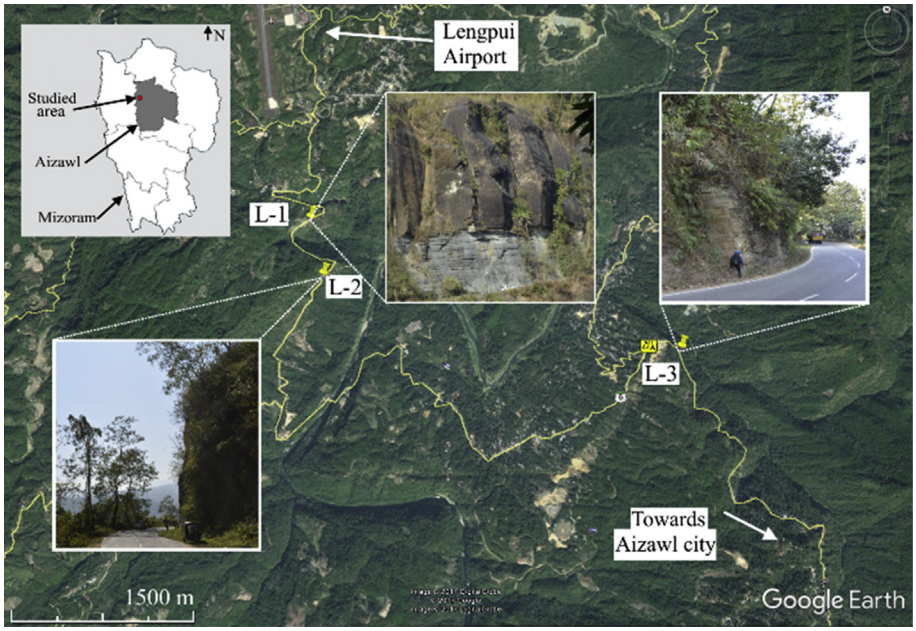

Fig. 1. Map of the study area (modified Google Earth imagery).

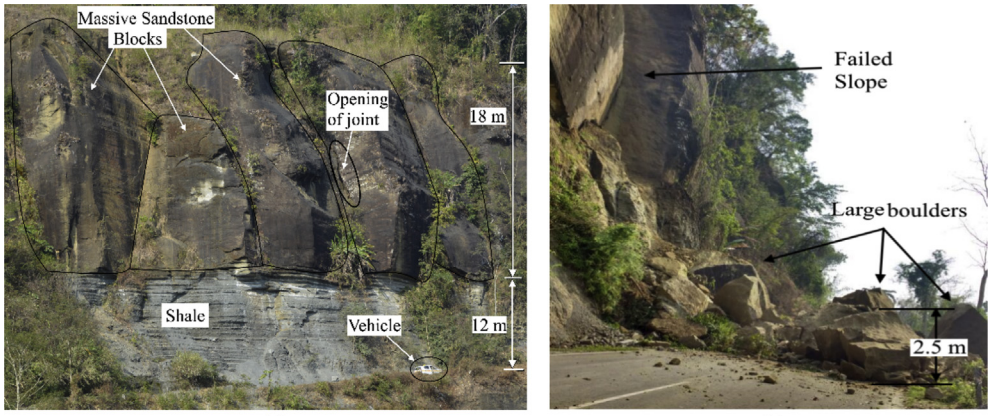

Fig. 2. Field photographs of location L-1 showing (a) Rock slope before failure (photograph taken in January 2017) and (b) Failed slope and blocked highway due to falling of large boulders (photograph taken in April 2017).

'A' rated slopes has been evaluated by following the preliminary rating of five rock slopes based on RHRS method. The kinematic analysis has been used in the study to identify the type of failure. The instability or weakest section in the slope, size and type of failure, and rockfall initiation point have been found in 3D stability analysis. The rockfall analysis has been carried out for the slope which is instable or has RHRS score more than 500, as given in flowchart showing the methodology used (Fig. 3).

3.1. Rockfall hazard assessment

3.1.1. Preliminary rating

RHRS is a qualitative assessment method of rockfall vulnerability along the road cut slopes for the assessment of rockfall hazards. It is a proactive system which consists of preliminary rating and detailed rating of slopes. Initially, five slopes have been analyzed along the highway NH-44A for preliminary rating and the slopes were rated high/moderate/low class (i.e. category A, B or C) on the basis of two criteria, i.e. 'estimated potential for rockfall on roadway' and 'historical rockfall activity' (Pierson and Van Vickle, 1992; Pierson et al., 2005). Estimated size or volume of material and ditch effectiveness have been considered during the former rating criterion whereas the frequency of rockfall and size or volume of rock blocks falling from the slope have been considered in the rating of later criterion. The risks of 'A, B and C' rated slopes are moderate to high, low to moderate and non-existent to low, respectively. In the present study, the L-1 slope has very large size or volume of rock blocks to fall out with a history of rockfall whereas L-2 and L-3 slopes have a potential of falling rock block size of 2–3 ft (1 ft = 30.48 cm) but they also retain a history of rockfall on the roadway. The locations L-4 and L-5 exhibit lower size of rock blocks and do not have any rockfall history. Thus 'A' category has been assigned to L-1, L-2 and L-3 slopes and the remaining two slopes have been assigned as 'C' category in the preliminary rating. The purpose of the preliminary rating is to prioritize the slope for evaluation of detailed rating.

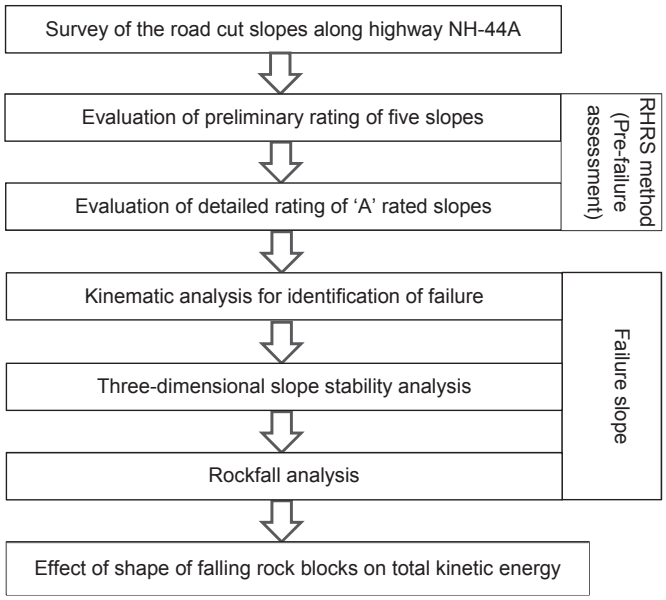

Fig. 3. Methodology of the study.

3.1.2. Detailed rating

In the detailed rating, the studied slope has been evaluated and scored on the basis of nine categories which define the significance of parameters in the contribution of rockfall hazard. On the basis of evaluation, each category has been scored from 1 to 100 (Pierson and Van Vickle, 1993). The category scores have been added to calculate the total RHRS score for the studied slope. The rating of each category is based on an exponential scale, which implies that for a more hazardous parameter, the category score will increase exponentially on the basis of Eq. (1):

$$y = 3^x \tag{1}$$

where x is the category specific exponential function, for some of the categories, its value can be measured from the formulae given in Table 1 and the remaining categories which are not associated with any formula can also exponentially increase based on RHRS manual.

The slope height can be directly measured from the field location and scored on the basis of relationship provided in Table 1 and Eq. (1). The effectiveness of the ditch can be evaluated on the basis of width, depth and shape of the ditch, and slope height and angle. The average vehicle risk (AVR) can be calculated by

$$AVR = \frac{(ADT/24)L_S}{S} \times 100\% \tag{2}$$

where ADT is the average daily traffic expressed in cars per day, L_S is the length of slope in km, 24 is the number of hours per day, and S is the speed limit in km/h. The percentage of decision sight distance (PDSD) can be calculated by

$$PDSD = \frac{ASD}{DSD} \times 100\% \tag{3}$$

where ASD is the actual sight distance in km. It is a distance that a driver's eyes (i.e. height of 3.5 ft from the ground) need to see the existence of an unknown object of 6 in (1 in = 2.54 cm) on the road (AASHTO, 1994). DSD is the decision sight distance expressed in km and its value is calculated on the basis of a speed limit of the area according to the procedure described by AASHTO (2004). Similarly to the slope height, road width has been measured at the field location.

The geological character is further categorized into two cases. Case-I includes 'structurally controlled' rockfalls and Case-II includes rockfalls due to 'differential erosion'. Generally, both cases are measured simultaneously and the highest scored case is considered in the calculation of final RHRS score. In the next category, expected rock block size or volume per rockfall event is evaluated and scored according to Table 1 and Eq. (1). The highest scored category between rock block size and block volume is considered for the final scoring. The three main factors for the evaluation of climate conditions are rainfall, freeze–thaw cycle and groundwater circulation. These are the qualitative factor and can be scored as per Table 1 and Eq. (1). Rockfall history is the last category, which is basically the past activity of rockfall or historical database and is used to know whether few, occasionally, many or constant falls occur.

Table 1
Exponential formulae for calculation of RHRS score (Pierson et al., 2005).

Parameter	Unit	Exponential formula
Slope height (H_S)	ft	$x = H_S/25$
Average vehicle risk (AVR)	%	$x = AVR/25$
Percentage of decision sight distance (DSD)	%	$x = (120-DSD)/20$
Road width (W_R)	ft	$x = (52-W_R)/8$
Block size (S_B)	ft	$x = S_B$
Volume of rockfall per event (V_B)	cubic yard	$x = V_B/3$
Annual rainfall (AR)	in	$x = AR/10$

3.2. Kinematic analysis

During the field survey of slope L-1, three types of joint sets have been identified with a dip and dip direction of joint J1 (89°/135°), joint J2 (87°/52°) and bedding J3 (7°/328°). The weathering of sandstone blocks varied from slight to moderate, whereas for shale, it was moderate to high. The roughness has been observed to vary from slickenside to slightly rough for sandstone block and moderate for shale. In the kinematic analysis, the stereographic projection found that the wedge failure is present. The wedge is formed due to an intersection of joints J1 and J2 which lies in the critical zone (Fig. 4a). The trend (α_i) and plunge (β_i) are found to be 62° and 80°, respectively, for wedge failure in the kinematic analysis. A similar type of wedge failure has been observed in the field which supports the result of the kinematic analysis (Fig. 4b).

3.3. Geometry and material properties

3.3.1. 3D numerical simulation

The 3D numerical simulation has been performed to analyze the stability of jointed rock slope using 3DEC (Itasca, 2016). It has the ability to simulate the jointed rock mass behavior by assuming joint as a boundary condition between the intact rock blocks; large displacement along the joint and rotation of the block are allowed.

The geometry used in the numerical model for rock slope is shown in Fig. 5. Joint sets A and B were explicitly included in the numerical model, requiring their properties to be treated separately. The properties of intact sandstone blocks used for numerical simulation are given in Table 2. Joint properties, for instance, dip, dip direction, cohesion and internal friction angle used in the numerical model, were collected from field observation and previously published literature (Barton, 1976; Gischig et al., 2011). The behavior of the discontinuity sets is modeled using Mohr-Coulomb slip model with residual strength. Intact rock bridges along large-scale discontinuities were modeled indirectly by assigning higher

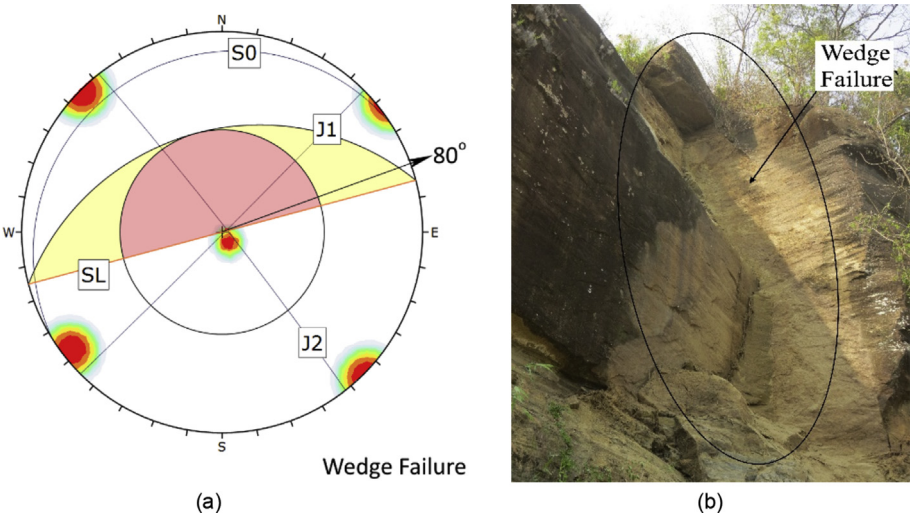

Fig. 4. (a) Stereographic projection showing wedge failure in the kinematic analysis, and (b) Photograph showing wedge failure in the field.

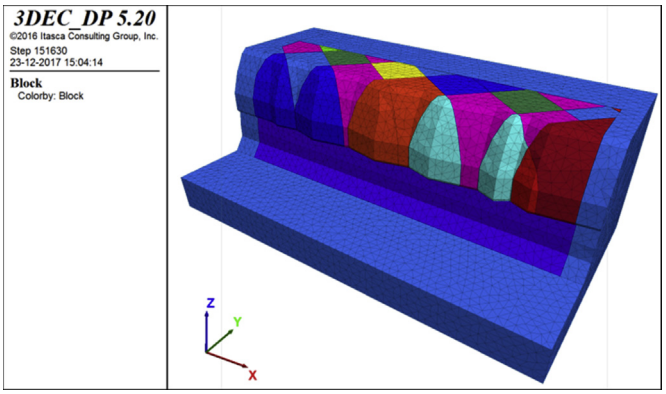

Fig. 5. 3D geometry and joint mapping of the slope.

Table 2
Block and joint properties used in the 3DEC simulation.

Material	Input parameter	Value	Unit
Intact sandstone block	Density	2700	kg/m^3
	Bulk modulus	12.74	GPa
	Shear modulus	8.39	GPa
	Cohesion	5.5	MPa
	Internal friction angle	36	°
	Tensile strength	2.5	MPa
Joint J1	Dip	85	°
	Dip direction	135	°
	Spacing	6–8	m
	Joint normal stiffness	3.32	GPa/m
	Joint shear stiffness	1.2	GPa/m
	Internal friction angle	32	°
	Cohesion	0.1–0.6	MPa
Joint J2	Dip	89	°
	Dip direction	219	°
	Spacing	4–6	m
	Joint normal stiffness	3.32	GPa/m
	Joint shear stiffness	1.2	GPa/m
	Internal friction angle	32	°
	Cohesion	0.1–0.6	MPa

initial strength properties to discontinuities, as described by Jennings (1970) and recently applied by Fischer et al. (2010). The discontinuity strength parameter, basically the friction angle, was derived from published data of strength tests (Kulhawy, 1975) based on field observations of the joint characteristics (surface roughness, alteration, etc.). For joint cohesion, a range of values were tested to account for varying assumptions regarding the role of shear resistance provided by intact rock bridges. As a starting point, initial values were based on those recommended by Wyllie and Mah (2014) for discontinuities in hard rock (cohesion ranging from 0 to 100 kPa). These values were then adjusted for the field conditions and a value was selected which represents nearly the similar behavior as the field slope. The joint properties like joint stiffness were evaluated from rock mass properties. The normal and shear stiffnesses of joints were estimated from rock mass deformation modulus, intact rock Young's modulus and mean joint spacing with the help of Eq. (4):

$$k_n = \frac{E_i E_m}{L(E_i - E_m)} \tag{4}$$

where k_n is the joint normal stiffness, E_m is the rock mass modulus, E_i is the intact rock modulus, and L is the mean joint spacing.

Similarly, the joint shear stiffness can be evaluated by

$$k_s = \frac{G_i G_m}{L(G_i - G_m)} \tag{5}$$

where k_s is the joint shear stiffness, G_m is the rock mass shear modulus, and G_i is the intact rock shear modulus.

3.3.2. Determination of coefficient of restitution in the laboratory

The coefficient of restitution (COR) plays an important role in the analysis of the rockfall. It is associated with the energy dissipation during the impact. The normal coefficient of restitution (R_n) has been calculated in the laboratory using fabricated setup (Fig. 6a). The experimental setup consists of a steel frame with a releaser fixed at the top and a casing at the base for accommodating the rock slab. The height of the releaser can be varied by adjusting the threaded rod attached to it. The supporting frame is mounted along with a scale of 1-m length graduated in millimetre. The angle of the resting slab can be varied by adjusting the pinion attached to the base frame (Fig. 6a). A high-speed camera is used for image exposures in excess of 1/1000 or frame rates in excess of 250 frames per second. It is used to record fast-moving objects as a photographic image(s) onto a storage medium. After recording, the images stored on the medium can be played back in slow-motion.

The rock slab has been placed under the sample holder and a high-speed camera was fixed parallel to the setup. The small rock

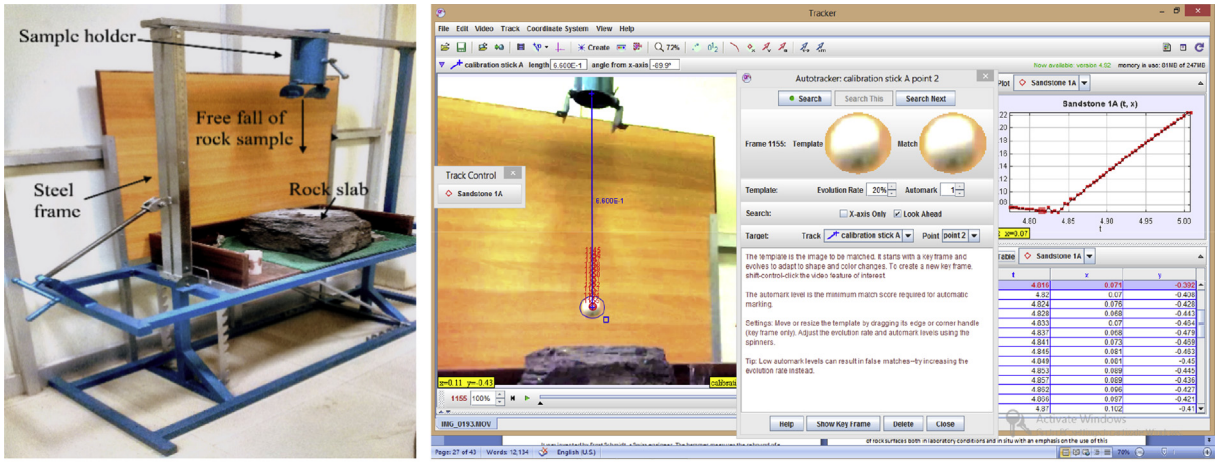

Fig. 6. (a) Fabricated experimental setup for COR, and (b) Tracking of sample and tabulation of data.

Table 3
Normal coefficient of restitution values for sandstone and shale.

Sample	V_i (m/s)	V_f (m/s)	R_n	Average of R_n
Sandstone 1	3.63	1.66	0.457	0.453
Sandstone 2	3.59	1.56	0.435	
Sandstone 3	3.64	1.69	0.466	
Shale 1	3.56	1.68	0.472	0.467
Shale 2	3.58	1.66	0.463	
Shale 3	3.62	1.69	0.466	

sample was kept in the holder and released such that it experienced a free fall and bounce on the rock slab. The motion was captured by the camera and the procedure was repeated for three samples of sandstone and shale each. Later the recorded video was transferred to the computer and analyzed by the motion tracking software (Fig. 6b). The tabulated data were analyzed after the required bounce of the sample was tracked in the software. The velocity variation graph has been generated by the software. The maximum positive value of V_f and the maximum negative value of V_i are taken to calculate R_n as follows:

$$R_n = \frac{V_f}{V_i} \tag{6}$$

where V_f and V_i are the final and initial velocities of the falling rock block bounces on the rock slab, respectively. The average values of R_n for sandstone and shale are calculated to be 0.45 and 0.47, respectively, from Table 3.

3.3.3. Rockfall geometry

The geometry of the slope has been generated to present the actual scenario of the studied slope in the best possible approximation (Fig. 7a). On the basis of the survey of the studied slope, the model has been divided into bedrock and asphalt. The upper and lower parts of the slope were observed to be sandstone and shale, respectively. The total height of 30 m of the slope included 12 m of shale and 18 m of sandstone, and the width of the roadway has been measured as 8 m in the field. The values of tangential COR (R_t), dynamic friction and rolling resistance has been taken from the COR table provided by the Rocscience. In the analysis, it has been found that the motion of falling rock block is observed to be the roll, fall and bounce.

The rigid mass formulation has been considered in the analysis due to their sensitivity towards the shape of rock block. Different shapes and sizes of the rock blocks in the rockfall model can change the contact kinematics and impact dynamics (Dadashzadeh et al., 2014). Unlike the lumped mass formulation, rigid mass formulation allows a user to select any shape and size of falling rock blocks. The values of normal (R_n) and tangential CORs (R_t) and other input parameters are given in Table 4. Based on the pre-failure and post-failure survey of the studied slope and the findings of the 3D stability analysis, the location of seeder has been taken in the rockfall model. Two point seeders (S1 and S2) and one line seeder (S3) have been considered in the analysis of rockfall: the first detachment point (S1) at the height of 29.3 m near the crest of the slope, the second detachment point (S2) at the height of 6.7 m on the lower portion of the sandstone, whereas the line seeder (S3) has been considered on the lower front side of the sandstone (Fig. 7a). The seeders have been assigned the average mass of 5 t, 10 t, 15 t and 20 t. The dimensions of the boulder that stopped in the middle of the roadway are measured to be 2.5 m × 1.5 m × 1 m, as shown in Fig. 7b. The shapes of the rock blocks considered in the analysis are triangular, rhomboid, pentagonal, hexagonal and octagonal as per post-failure survey (Fig. 7c). Each seeder has been assigned to 400 rock blocks (i.e. totally 1200 falling rock blocks).

4. Results and discussion

4.1. RHRS method

The slope heights (H_S) and roadway widths (W_R) for locations L-1, L-2 and L-3 were measured to be 100 ft, 33 ft, 40 ft and 27 ft, 27 ft, 23 ft, respectively. With the use of above discussed exponential formulae in Table 1 and Eq. (1), the slope height and roadway width categories are scored for all three studied slopes. The kinetic energy of falling rock block increases with increase in slope height and the higher roadway width helps the driver to react and take an action in case of rockfall event occurred. Thus the higher slope height and the lesser roadway width make the slope more hazardous. The ditches are cost-effective catchment area to arrest the falling rock blocks. No ditch was found at any of the studied locations and the gap between the toe of the slope and the edge of the roadway was observed to be ineffective to arrest the falling rock blocks. Hence, 'no catchment' has been assigned to this category. The AVR and PDSD have been calculated from the above-discussed exponential formulae. The value of ADT has been taken as 5000, the values of L_S

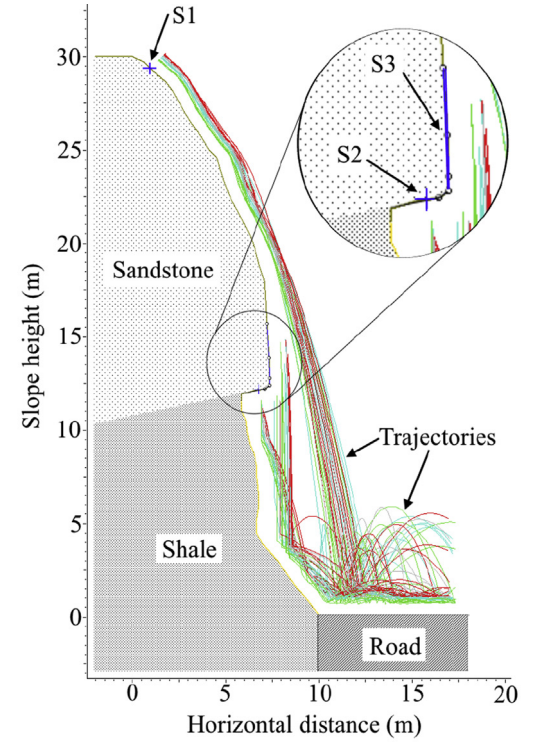

(a)

(b)

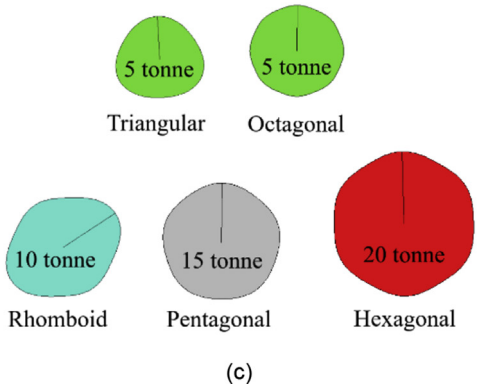

(c)

Fig. 7. (a) Rockfall model of the studied slope with the location of seeders, (b) Size of the falling boulder stopped in the middle of the roadway, and (c) Shapes and weights of the falling rock blocks from the seeders.

were measured as 100 m, 15 m and 45 m for locations L-1, L-2 and L-3, respectively, and the speed limit at the location was 50 km/h. The value of ASD has been measured as 70 m for location L-1 and 55 m for both locations L-2 and L-3. The value of DSD has been assumed as 145 m for the study area. AVR explains the average percentage time of presence of a vehicle in the rockfall-prone area. Its value can be more than 100% in case of high ADT and slope length. During the survey, the length of the joint has been observed to vary from 6 m to 20 m for all studied slopes. The joints longer than 3 m can be considered as continuous joints. In the geological character category, the structural condition has been observed as 'continuous joints' for all three locations. The rock friction affects the potential of movement of a rock block relative to another rock block. For slope L-1, the rock friction has been observed as 'slickensided' whereas for the remaining two locations, it has been observed as 'planar'.

Hoek (1999) stated that the slope with a rating less than 300 can be categorized as 'low urgency', 300–500 can be categorized as 'moderate urgency', and higher than 500 comes under 'higher urgency'. The rockfall hazard discloses that the one of three slopes has RHRS score more than 500 which implies that it is under 'higher urgency' and needs an immediate attention for treatment whereas the remaining two slopes L-2 and L-3 come under 'moderate urgency' and are prone to rockfall failure.

A histogram is plotted in Fig. 8, which shows the percentage contribution of each parameter in the overall RHRS score for all three locations. The maximum contribution in the total score has been provided by 'geological character' after combining its two parameters 'structural discontinuity' and 'rock friction' for all the studied slopes. The trend in the histogram for all locations is the same for all categories except 'slope height' and 'rock block/volume' due to the fact that the slope height and falling rock volume for L-1 have found to be greater than the other slopes. Thus, these categories made higher contribution to the total score of the slope L-1. The PDSD category shows the higher contribution of the slopes L-2 and L-3 due to the low value of ASD. The smaller the road width, the higher the rockfall vulnerability. The roadway width category for the slope L-3 shows higher contribution due to the undersized road width as compared to the other slopes. The lowest contribution (approximate 1% of the total score) was observed by 'average vehicle risk' category in all three locations due to the low traffic volume.

In the next category, the expected size of the rock block or/and the rock block volume per event has been evaluated and scored. Generally, the category with the highest score is considered in the final RHRS score but in the case of the slope L-1, both the categories, rock block size and rock block volume scored 100 as the large volume of rock block has been expected to fall out; thus either of any category can be considered in the final scoring sheet, whereas in the case of the slopes L-2 and L-3, the highest rating was calculated using rock block size. The large size or volume of the falling rock blocks produces the high impact forces and high kinetic energy, i.e. less safe for the vehicles. In addition, the path obstructed by larger rock blocks is more than that by lower rock blocks on the roadway. As all the studied slopes come under the same area, the climate conditions would be the same. The rainfall data show 100 in of rainfall per year which gives the maximum score of 100. Water or rainfall increases the weathering and movement of rock blocks from the slope surface, which causes the instability of the slope. There were no traces of freeze and thaw activities and no groundwater circulation at any of the studied locations, thus zero scores were assigned for these two parameters. The historical data of rockfall state that during the pre-monsoon and monsoon seasons, rockfall frequently occurs in this area. Hence this category has been assigned to 'many falls' with a score of

Table 4
Input parameters used in the rockfall analysis.

Slope material		R_n	R_t	Dynamic friction coefficient	Rolling resistance coefficient
Sandstone		0.45 (±0.04)	0.85 (±0.04)	0.5 (±0.04)	0.15 (±0.02)
Shale		0.47 (±0.04)	0.85 (±0.04)	0.5 (±0.04)	0.15 (±0.02)
Asphalt (roadway)		0.4 (±0.04)	0.9 (±0.04)	0.5 (±0.04)	0.1 (±0.01)
Parameter		Value		Unit	
Initial conditions	Horizontal velocity	0		m/s	
	Vertical velocity	0		m/s	
	Rotational velocity	0		°/s	
Density		2700		kg/m^3	
Average mass of rock block		5, 10, 15, 20		t	
Shapes of rock block		Triangular, rhomboid, pentagonal, hexagonal and octagonal			
Number of falling rock blocks considered		1200 (300 for each mass)			
x and y coordinates of seeders	Point S1	(0.9, 29.3)		m	
	Point S2	(6.7, 12.1)		m	
	Line S3	(7, 12.2) to (7.1, 15.8)		m	
Gradient of slope		80–90		°	

Note: The values in the brackets such as ±0.04 represent the standard deviation.

27 for all three locations. This category represents the known rockfall event at the studied locations. This datum can be used as important information for future rockfall events on the slope. The total RHRS scores of 639, 451 and 486 have been obtained by addition of each category scores for locations L-1, L-2 and L-3, respectively (Table 5).

4.2. Displacement and velocity of blocks using distinct element method

The maximum displacement of 2.24 cm has been found in the numerical simulation for one of the five sandstone blocks (i.e. the first block from the right side, as shown in Fig. 9a). The size of this block is smaller as compared to that of other four blocks due to reduced joint spacing, but it has more hanging volume in the air which makes it least stable among all the blocks. The maximum velocity observed for this particular block is 2.25 mm/s. The numerical velocity plot is used to identify the areas which are either stable or undergoing failure (Fig. 9b). The values which are close to zero in numerical velocity plot indicate the stable region. It has been observed from the results that the regions of high velocity, corresponding to those of high displacement, show the instability of blocks. The high values of velocity and displacement of five blocks illustrate that the blocks are unstable and vulnerable to rockfall activity. The results from the numerical simulations were found similar to the field observation after the block failure from the slope L-1, as shown in Fig. 9c. The region with the high displacement value is further used as rockfall initiation point in the rockfall simulation.

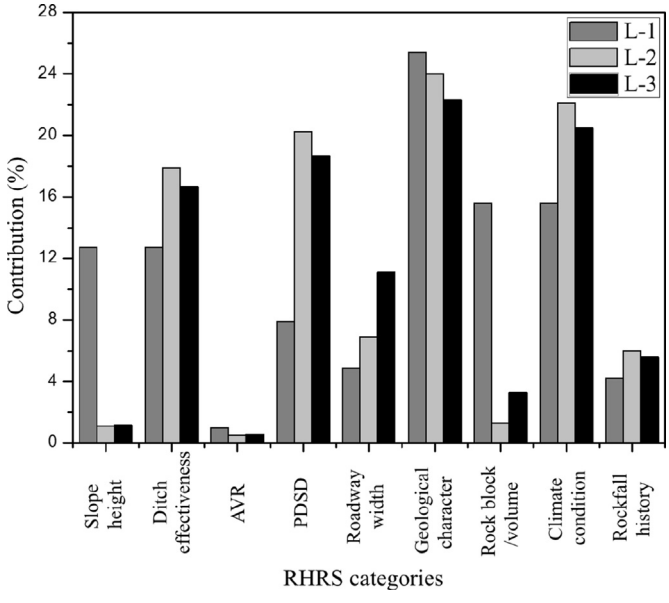

Fig. 8. Contribution of each category score in the overall RHRS score.

4.3. Rockfall simulation of failed slope

4.3.1. Run-out distance and bounce height

The rockfall analysis reveals that the falling rock blocks of different masses and shapes from the cliff are scattered on the roadway (and some of them further fall into the valley). In the rockfall model, the width of the roadway was taken as 8 m (i.e. horizontal distance from 10 m to 18 m). It was observed that 25% of rock blocks stopped on the roadway before reaching the other end of the roadway (Fig. 10a). The minimum run-out distance observed during the analysis was 10.6 m whereas the maximum run-out was up to the valley. The maximum run-out distance implies that the whole width of the roadway is unsafe

Table 5
Rockfall hazard rating criteria and score for the studied locations (Pierson and Van Vickle, 1992).

Category	Sub-category	Score		
		L-1	L-2	L-3
Slope height		81	5	6
Ditch effectiveness		81	81	81
AVR		6	2	3
Percentage of PDSD		51	91	91
Road width		31	31	54
Geological character	Structural condition	81	81	81
	Rock friction	81	27	27
Block size/volume per event		100	6	16
Climate conditions	Rainfall	100	100	100
	Freeze and thaw	0	0	0
	Groundwater circulation	0	0	0
Rockfall history		27	27	27
Total RHRS score		639	451	486

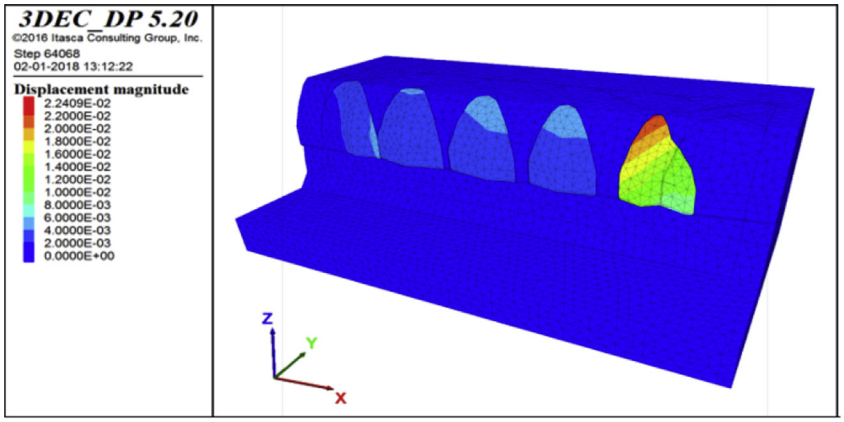

(a)

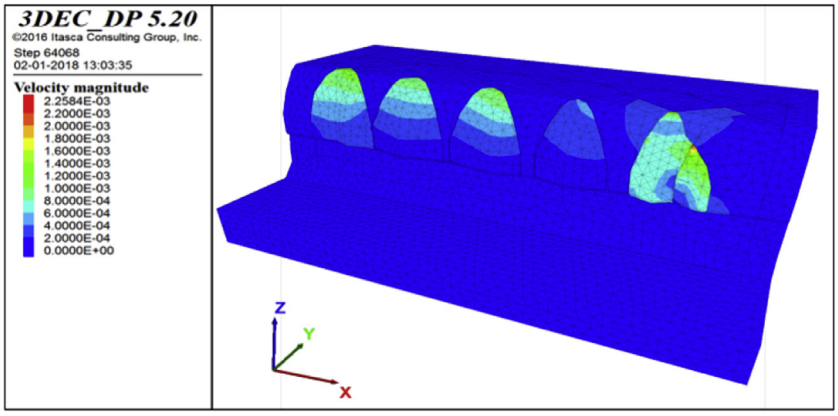

(b)

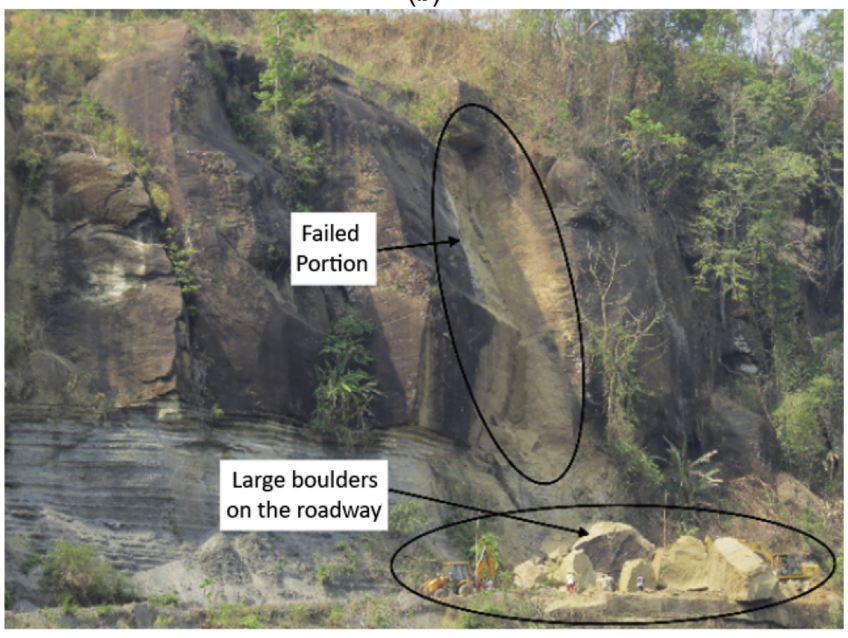

(c)

Fig. 9. (a) Total displacement contours (m), (b) Contours of the velocity of the blocks (m/s), and (c) Rock slope after failure (photograph was taken in April 2017).

and the falling rock blocks can cause damage to the vehicles on that road.

The bounce height is one of the many important parameters in the rockfall analysis, which is affected by the slope geometry, slope gradient, shape and size of falling rock blocks. The maximum bounce height observed during the analysis was in the range of 5.3–6.9 m for different masses of falling rock blocks on the roadway (Fig. 10b). From the seeder S1, the

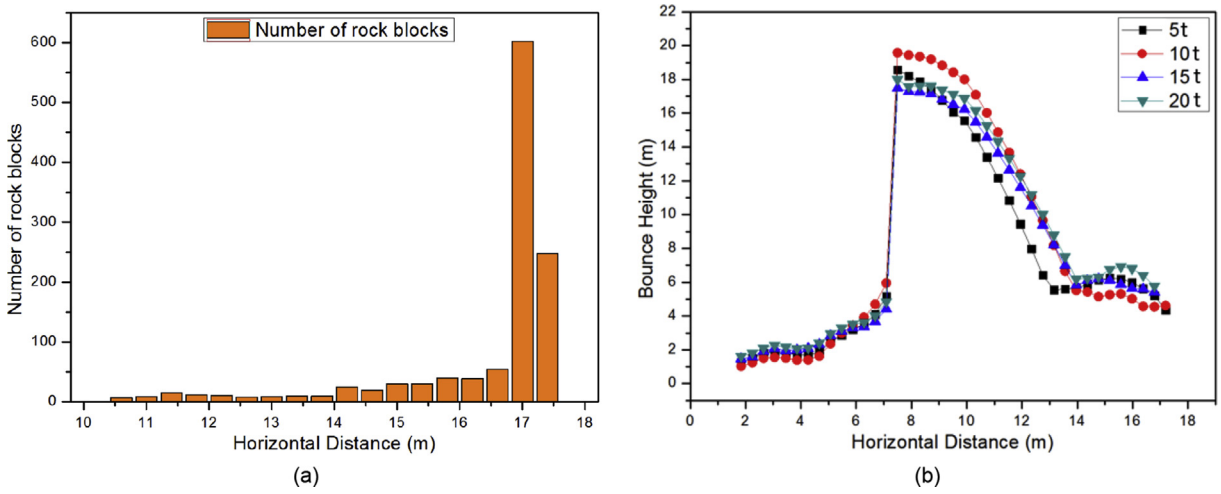

Fig. 10. (a) Run-out distance of falling rock blocks and (b) Bounce height on the slope and the roadway.

motion of the falling rock block was observed as roll-fall-bounce-roll. The rock block starts to roll, fall from the cliff and bounce on the roadway, whereas in seeders S2 and S3, the rock block starts to fall from the cliff, bounce on the lower portion of the slope (i.e. shale) and then again bounce on the roadway. At the horizontal distance of 6.7–7.1 m, there is a sudden rise in bounce height up to 17 m due to the falling motion of rock blocks from the seeder S1 (Fig. 10b).

4.3.2. Total kinetic energy and translational velocity

When the rock block detaches from the slope, the potential energy is converted into kinetic energy. The vertical component of velocity is increased due to the gravity effect on the rock block which results in increased kinetic energy. The mass of the rock block is another parameter which affects the kinetic energy, i.e. the greater the mass, the higher the kinetic energy (Fig. 11a). The increase in kinetic energy has been observed during the fall from the slope and decrease in its value was observed after several numbers of the impact of rock blocks on the roadway. The maximum kinetic energy was found to be 5047 kJ for a mass of 20 t whereas it was 1246 kJ for a mass of 5 t on the roadway. This amount of energy is large enough to destroy the vehicle or to disrupt the traffic for several days.

The factors which affect the translational velocity are the height of the slope, angle of slope and the frictional coefficient of the slope material. The trend shows that due to the falling of rock blocks from the slope surface, the translational velocity increases initially and then decreases at a horizontal distance of 14 m due to many bounces on the roadway (Fig. 11b). The maximum translational velocity was observed to be 22.2 m/s and 22.4 m/s for a mass of 20 t and 5 t, respectively.

The maximum values observed in the analysis for all the parameters such as bounce height, run-out distance, translational velocity and total kinetic energy are given in Table 6. For four different masses (i.e. 5 t, 10 t, 15 t and 20 t), the maximum bounce height on the roadway has been observed between the horizontal distances of 14 m and 16 m. Both the maximum translational velocity and the kinetic energy on the roadway have been observed between the horizontal distances of 11.5 m and 12.7 m. The maximum run-out distance has been observed up to the valley side.

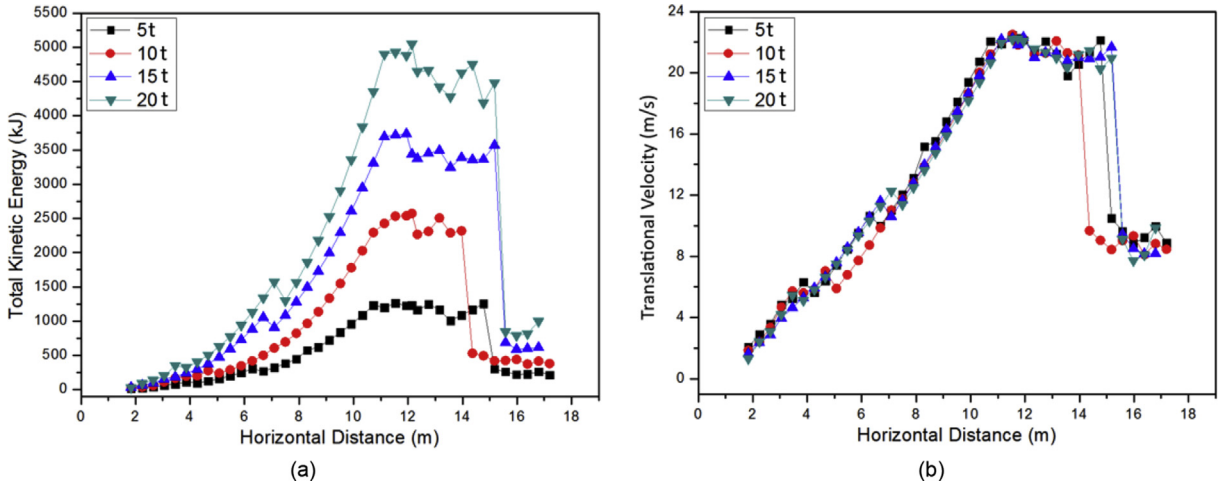

Fig. 11. (a) Total kinetic energy and (b) Translational velocity on the slope and the roadway.

Table 6
Parameters obtained from the rockfall analysis along NH-44A.

Mass (t)	Maximum bounce height (m)	Maximum translational velocity (m/s)	Maximum total kinetic energy (kJ)	Maximum run-out distance (m)
5	6.2	22.4	1230	18
10	5.3	22.5	2539	18
15	6.1	22.2	3734	18
20	6.9	22.2	5047	18

difference between the kinetic energies of the triangular and hexagonal shapes of rock blocks has been observed. On the basis of higher to lower energy generated during fall of rock blocks, the order of its shape is rhomboid, hexagonal, triangular, pentagonal and octagonal. Fig. 12b shows the effect of the shape (triangular, rhomboid, pentagonal, hexagonal and octagonal) of the rock block with a mass of 20 t on the total kinetic energy of the falling rock block.

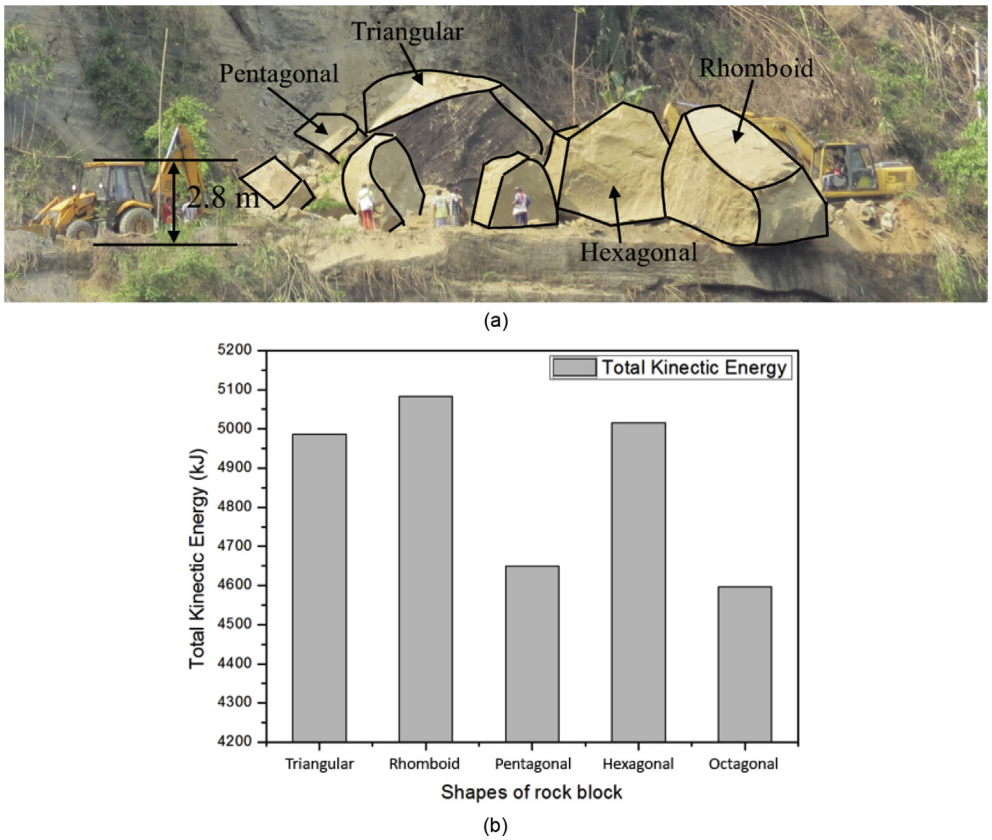

Fig. 12. (a) Boulders of different shapes and sizes at the edge of a roadway on valley side, and (b) Effect of shape of rock block on total kinetic energy.

4.4. Effect of shape of the rock block on the total kinetic energy

Different shapes and sizes of the falling rock blocks change the contact points and the impact forces between the falling rock block and the surface of the slope (Vijayakumar et al., 2011) which affect the trajectory, run-out distance, velocity and kinetic energy of falling rock blocks. Different shapes (triangular, rhomboid, pentagonal and hexagonal) of rock blocks fell down during the failure of slope L-1 (Fig. 12a). The large boulders of approximate 3 m in height blocked the NH-44A. The effect of the shape of rock blocks on kinetic energy has been observed in this study. In the rockfall analysis, it has been found that rhomboidal rock blocks possess a high amount of kinetic energy (i.e. 5047 kJ) as compared to other shapes whereas octagonal rock blocks possess 4597 kJ of energy, which has been found to be a minimum amount of kinetic energy for a mass of 20 t. The small

5. Conclusions

Rockfall hazard assessment has been carried out to identify the hazardous slopes on the NH-44A. It reveals that the one out of three studied slopes was highly prone to rockfall (i.e. RHRS score >500) and posed a threat to the vehicles and passer-by. Five massive sandstone blocks were lying on shale bedding before the rockfall activity occurred on slope L-1. Though a portion of the L-1 has already fallen down, but to prevent the failure of the remaining massive blocks, the remedial measure is needed on a highly urgent basis. The rockfall event has occurred within the three months of the detailed survey. The geological condition, differential weathering and high intensity of pre-monsoon rainfall were the causes of rockfall activity on the studied location. The joint opening on the massive sandstone block near the failure portion of the slope as shown in Fig. 2a makes it more vulnerable as compared to other massive sandstone blocks.

The discontinuum analysis was carried out for better understanding of the failure mechanism, geometry of the failure surfaces, effect of joint parameters and rockfall vulnerable zones (unstable blocks) for slope. This study can be useful for forecasting rock slope movement and adoption of safety measures against rockfall activity. The primary cause of the failure was wedge formation by joint sets J1, J2 and J3. Numerical results show the maximum values of displacement and velocity for the failed block, mainly due to particular shape and size of the block. The numerical results verify the findings of the kinematic analysis as well as the post-failure scenario of the slope.

The study concluded that the whole width of the roadway was unsafe as the falling rock blocks either stopped on the roadway or fell into the valley (Fig. 10a). After the slope failure, the highway was blocked and some of the rock blocks fell into the valley (Fig. 2b). The high kinetic energies were associated with the large size of falling rock blocks (i.e. size >2.5 m), which is quite enough to break down any structure or vehicle or can cause fatalities. The results of rockfall simulation are found similar to the post-failure observations in the field.

Conflicts of interest

The authors wish to confirm that there are no known conflicts of interests associated with this publication and there has been no significant financial support for this work that could have influenced its outcome.

Acknowledgments

The authors would like to thank the Ministry of Earth Sciences, Government of India (MoES/P.O(Geosci)/42/2015) for the grant to carry out this study.

References

Ahmad M, Umrao RK, Ansari MK, Singh R, Singh TN. Assessment of rockfall hazard along the road cut slopes of state highway-72, Maharashtra, India. Geomaterials 2013;3(1):15–23.
Agliardi F, Crosta GB. High resolution three-dimensional numerical modelling of rockfalls. International Journal of Rock Mechanics and Mining Sciences 2003;40(4):455–71.
AASHTO. A policy on geometric design of highways and streets. Washington: American Association of State Highway and Transportation Officials (AASHTO); 1994.
AASHTO. A policy on geometric design of highways and streets (the green book). Washington: AASHTO; 2004.
Ansari MK, Ahmad M, Singh R, Singh TN. Rockfall assessment near saptashrungi gad temple, Nashik, Maharashtra, India. International Journal of Disaster Risk Reduction 2012;2:77–83.
Ansari MK, Ahmad M, Singh R, Singh TN. Rockfall hazard rating system along SH-72: a case study of Poladpur-Mahabaleshwar road (Western India), Maharashtra, India. Geomatics, Natural Hazards and Risk 2016;7(2):649–66.
Barton N. The shear strength of rock and rock joints. International Journal of Rock Mechanics and Mining Sciences & Geomechanics Abstracts 1976;13(9):255–79.
Brawner CO, Wyllie D. Rock slope stability on railway projects. Area Bulletin 1976;656:449–74.
Budetta P. Assessment of rockfall risk along roads. Natural Hazards and Earth System Science 2004;4(1):71–81.
Cruden DM, Varnes DJ. Chapter 3-Landslide types and processes. In: Landslides: investigation and mitigation. Transportation Research Board; 1996. p. 36–75.
Cundall PA. Formulation of a three-dimensional distinct element model. Part I. A scheme to detect and represent contacts in a system composed of many polyhedral blocks. International Journal of Rock Mechanics and Mining Sciences & Geomechanics Abstracts 1988;25(3):107–16.
Dorren LK. A review of rockfall mechanics and modelling approaches. Progress in Physical Geography 2003;27(1):69–87.
Dorren LK, Berger F, Putters US. Real-size experiments and 3-D simulation of rockfall on forested and non-forested slopes. Natural Hazards and Earth System Sciences 2006;6(1):145–53.
Dadashzadeh N, Duzgun HS, Yesiloglu-Gultekin N, Bilgin A. Comparison of lumped mass and rigid body rockfall simulation models for the Mardin Castle, Turkey. In: Proceedings of the 48th US rock mechanics/geomechanics symposium. American Rock Mechanics Association; 2014.
Douglas GR. Magnitude frequency study of rockfall in Co. Antrim, N. Ireland. Earth Surface Processes and Landforms 1980;5(2):123–9.
Evans SG, Hungr O. The assessment of rockfall hazard at the base of talus slopes. Canadian Geotechnical Journal 1993;30(4):620–36.
Fell R, Corominas J, Bonnard C, Cascini L, Leroi E, Savage WZ. Guidelines for landslide susceptibility, hazard and risk zoning for land use planning. Engineering Geology 2008;102(3):85–98.
Ferrari F, Giacomini A, Thoeni K. Qualitative rockfall hazard assessment: a comprehensive review of current practices. Rock Mechanics and Rock Engineering 2016;49(7):2865–922.
Fischer L, Amann F, Moore JR, Huggel C. Assessment of periglacial slope stability for the 1988 Tschierva rock avalanche (Piz Morteratsch, Switzerland). Engineering Geology 2010;116(1–2):32–43.
Gischig V, Amann F, Moore JR, Loew S, Eisenbeiss H, Stempfhuber W. Composite rock slope kinematics at the current Randa instability, Switzerland, based on remote sensing and numerical modeling. Engineering Geology 2011;118(1–2):37–53.
Guzzetti F, Carrara A, Cardinali M, Reichenbach P. Landslide hazard evaluation: a review of current techniques and their application in a multi-scale study, Central Italy. Geomorphology 1999;31(1):181–216.
Guzzetti F, Reichenbach P, Ardizzone F, Cardinali M, Galli M. Estimating the quality of landslide susceptibility models. Geomorphology 2006;81(1–2):166–84.
Hoek E. Putting numbers to geology: an engineer's viewpoint. Quarterly Journal of Engineering Geology and Hydrogeology 1999;32(1):1–9.
Itasca. 3DEC - 3 dimensional discrete element code, Version 5.2, User's manual. Minneapolis, USA: Itasca Consulting Group Inc.; 2016.
Jennings JE. A mathematical theory for the calculation of the stability of slopes in open cast mines. In: Proceedings of the planning open pit mines. A.A. Balkema; 1970. p. 87–102.
Jin F, Zhang C, Hu W, Wang J. 3D mode discrete element method: elastic model. International Journal of Rock Mechanics and Mining Sciences 2011;48(1):59–66.
Kesari GK. Geology and mineral resources of Manipur, Mizoram, Nagaland and Tripura. Geological Survey of India, Government of India; 2011. Publication No. 30.
Kumar N, Verma AK, Sardana S, Sarkar K, Singh TN. Comparative analysis of limit equilibrium and numerical methods for prediction of a landslide. Bulletin of Engineering Geology and the Environment 2018;77(2):595–608.
Kundu J, Sarkar K, Tripathy A, Singh TN. Qualitative stability assessment of cut slopes along the National Highway-05 around Jhakri area, Himachal Pradesh, India. Journal of Earth System Science 2017;126(8):112.
Kulhawy FH. Stress deformation properties of rock and rock discontinuities. Engineering Geology 1975;9(4):327–50.
Lallianthanga RK, Lalbiakmawia F, Lalramchuana F. Landslide hazard zonation of Mamit town, Mizoram, India using remote sensing and GIS techniques. International Journal of Geology, Earth and Environmental Sciences 2013;3(1):148–94.
Matsuoka N, Sakai H. Rockfall activity from an alpine cliff during thawing periods. Geomorphology 1999;28(3–4):309–28.
McCarroll D, Shakesby RA, Matthews JA. Spatial and temporal patterns of late Holocene rockfall activity on a Norwegian talus slope: a lichenometric and simulation-modeling approach. Arctic and Alpine Research 1998;30(1):51–60.
Perret S, Dolf F, Kienholz H. Rockfalls into forests: analysis and simulation of rockfall trajectories - considerations with respect to mountainous forests in Switzerland. Landslides 2004;1(2):123–30.
Pierson LA, Davis SA, Van Vickle R. Rockfall hazard rating system implementation manual. Federal highway administration report No. FHWA-OR-EG-90-01. United States Department of Transportation; 1990.
Pierson LA, Van Vickle R. Rockfall hazard rating system. Transportation Research Record 1992;(1343):6–13.
Pierson LA, Van Vickle R. Rockfall hazard rating system: participants' manual. Report No. FHWA-SA-93-057. Federal Highway Administration; 1993.
Pierson LA, Beckstrand DL, Black BA. Rockfall hazard classification and mitigation system. Final Report No. FHWA/MT-05-011/8176. Montana Department of Transportation; 2005.
Ritchie AM. Evaluation of rockfall and its control. Highway Research Record 1963;(17):13–28.
Sardana S, Jha MK, Verma AK. Assessment of rockfall activity along the road cut slope in Himalayan region: a case study. In: Proceedings of the Indian geotechnical conference 2017. Indian Institute of Technology Guwahati; 2017.
Sardana S, Verma AK. Qualitative assessment of road cut slope in the northeast region of India - a case study. In: Proceedings of the 7th Indian rock conference; 2017. p. 284–9.
Sarkar K, Singh TN, Verma AK. A numerical simulation of landslide-prone slope in Himalayan region: a case study. Arabian Journal of Geosciences 2012;5(1):73–81.

Sarkar K, Singh AK, Niyogi A, Behera PK, Verma AK, Singh TN. The assessment of slope stability along NH-22 in Rampur-Jhakri Area, Himachal Pradesh. Journal of the Geological Society of India 2016;88(3):387–93.
Singh PK, Wasnik AB, Kainthola A, Sazid M, Singh TN. The stability of road cut cliff face along SH-121: a case study. Natural hazards 2013;68(2):497–507.
Singh TN, Verma AK. Evaluating the slope instability of the amiya slide. In: Proceedings of the 1st Canada-US rock mechanics symposium. American Rock Mechanics Association; 2007.
Valagussa A, Frattini P, Crosta GB. Earthquake-induced rockfall hazard zoning. Engineering Geology 2014;182:213–25.
Vandewater CJ, Dunne WM, Mauldon M, Drumm EC, Bateman V. Classifying and assessing the geologic contribution to rockfall hazard. Environmental and Engineering Geoscience 2005;11(2):141–54.
Varnes DJ. Landslide hazard zonation: a review of principles and practice. Paris: The UNESCO Press; 1984.
Verma AK, Singh TN. Assessment of tunnel instability: a numerical approach. Arabian Journal of Geosciences 2010;3(2):181–92.
Verma AK, Singh TN, Chauhan NK, Sarkar K. A hybrid FEM-ANN approach for slope instability prediction. Journal of the Institution of Engineers (India): Series A 2016;97(3):171–80.
Verma AK, Sardana S, Singh TN, Kumar N. Rockfall analysis and optimized design of rockfall barrier along a strategic road near Solang Valley, Himachal Pradesh, India. Indian Geotechnical Journal 2018. https://doi.org/10.1007/s40098-018-0330-6.
Vijayakumar S, Yacoub T, Curran J. A study of rock shape and slope irregularity on rock fall impact distance. In: Proceedings of the 45th US rock mechanics/geomechanics symposium. American Rock Mechanics Association; 2011.
Wang X, Zhang L, Wang S, Agliardi F, Frattini P, Crosta GB, Yang Z. Field investigation and rockfall hazard zonation at the Shijing Mountains Sutra caves cultural heritage (China). Environmental Earth Sciences 2012;66(7):1897–908.
Wei LW, Chen H, Lee CF, Huang WK, Lin ML, Chi CC, Lin HH. The mechanism of rockfall disaster: a case study from Badouzih, Keelung, in northern Taiwan. Engineering Geology 2014;183:116–26.
Wieczorek GF, Jager S. Triggering mechanisms and depositional rates of postglacial slope-movement processes in the Yosemite Valley, California. Geomorphology 1996;15(1):17–31.
Wieczorek GF, Nishenko SP, Varnes DJ. Analysis of rock falls in the yosemite valley, California. In: Daemen JJ, Schultz RA, editors. Proceedings of the 35th US symposium on rock mechanics. American Rock Mechanics Association; 1995. p. 85–9.
Wieczorek GF, Snyder JB, Waitt RB, Morrissey MM, Uhrhammer RA, Harp EL, Norris RD, Bursik MI, Finewood LG. Unusual July 10, 1996, rock fall at happy isles, yosemite national park, California. Geological Society of America Bulletin 2000;112(1):75–85.
Wyllie DC. Rock fall engineering. CRC Press; 2014.
Wyllie DC, Mah C. Rock slope engineering. CRC Press; 2014.
Zhang C, Hou Y, Jin F, Wang G, Zhang C. Analysis of arch dam-abutment stability by 3D deformable distinct elements. Chinese Journal of Rock Mechanics and Engineering 2006;25(6):1226–32 [in Chinese].

Dr. Amit Kumar Verma is currently Assistant Professor in the Department of Mining Engineering at prestigious Indian Institute of Technology (Banaras Hindu University), Varanasi. He has obtained his PhD from Indian Institute of Technology-Bombay and worked at several renowned institute across the world like 3S Laboratory, Grenoble, France and University of California Davis, USA. He was visiting faculty at Clausthal University of Technology, Germany and Endevour Executive Fellow at Monash University, Australia. He is recipient of prestigious awards like Institute of Engineers Young Engineers Award 2014–15, Inspire Faculty Fellowship 2012 by DST and INSA, Endevour Executive Fellowhip by Australian Government and Dr. K.S. Krishnan Research Associateship-24 in 2012 by Board of Research on Nuclear Sciences. Dr. Verma has published more than 70 papers in the field of Mining Engineering. He is member of reviewer board of several SCI journals.